

# Monitoring phase changes in supercooled aqueous solutions using an optical fiber Fresnel reflection sensor

Priyadarshini Mani,<sup>1</sup> Archana Rallapalli,<sup>1</sup> Venkata Rajanikanth Machavaram,<sup>1,3,\*</sup> and Akella Sivaramakrishna<sup>2</sup>

<sup>1</sup>*School of Electronics Engineering, VIT University, Vellore-632014, Tamilnadu, India*

<sup>2</sup>*School of Advanced Sciences, VIT University, Vellore-632014, Tamilnadu, India*

<sup>3</sup>*vr.machavaram@vit.ac.in*

*\*machavvr@aol.co.uk*

**Abstract:** We report on a technique for monitoring the crystallization of water and aqueous solution of NaCl at atmospheric pressure, when cooled via liquid nitrogen, using a Fresnel reflection-based optical fiber sensor. The crystallization of distilled water and the associated changes in refractive index inferred from the sensor response comply with the previous reports on physical properties of supercooled water. The phase separation of NaCl.2H<sub>2</sub>O and the formation of eutectic mixture were inferred from the distinct features of the sensor signal during the cooling of NaCl solution. But the thermocouple did not detect the exothermic heat of crystallization due to rapid cooling. The influence of temperature gradients while interpreting the optical signals during this rapid cooling process and the effects of sensor debonding during the heating phase are discussed. The results demonstrate the potential of Fresnel sensors for monitoring the crystallization-induced phase changes in supercooled salt solutions and offers applications in areas where monitoring and controlling crystallization is important.

©2016 Optical Society of America

**OCIS codes:** (060.0060) Fiber optics and optical communications; (060.2370) Fiber optics sensors; (010.7340) Water; (010.2940) Ice crystal phenomena.

---

## References and links

1. H. Kiani and D. W. Sun, "Water crystallization and its importance to freezing of foods: A review," *Trends Food Sci. Technol.* **22**(8), 407–426 (2011).
2. L. X. Yu, R. A. Lionberger, A. S. Raw, R. D'Costa, H. Wu, and A. S. Hussain, "Applications of process analytical technology to crystallization processes," *Adv. Drug Deliv. Rev.* **56**(3), 349–369 (2004).
3. X. Shi, M. Akin, T. Pan, L. Fray, Y. Liu, and Z. Yang, "Deicer impacts on pavement materials: Introduction and recent developments," *The Open Civil Eng. J.* **3**, 16–27 (2009).
4. R. W. Gent, N. P. Dart, and J. T. Cansdale, "Aircraft icing," *Phil. Trans.: Mathematical, Phys. and Eng. Sci.* **358**, 2873–2911 (2000).
5. P. G. Debenedetti, "Supercooled and glassy water," *J. Phys. Condens. Matter* **15**(45), R1669–R1726 (2003).
6. J. Y. Chen and C. S. Yoo, "High density amorphous ice at room temperature," *Proc. Natl. Acad. Sci. U.S.A.* **108**(19), 7685–7688 (2011).
7. P. W. Wilson, J. W. Arthur, and A. D. J. Haymet, "Ice premelting during differential scanning calorimetry," *Biophys. J.* **77**(5), 2850–2855 (1999).
8. M. A. Afromowitz and K. Y. Lam, "The optical properties of curing epoxies and applications to the fiber-optic epoxy cure sensor," *Sens. Actuat.* **A21**(1-3), 1107–1110 (1990).
9. P. A. Crosby, G. R. Powell, G. F. Fernando, C. M. France, R. C. Spooncer, and D. N. Waters, "*In situ* cure monitoring of epoxy resins using optical fibre sensors," *Smart Mater. Struct.* **5**(4), 415–428 (1996).
10. M. Giordano, A. Laudati, M. Russo, J. Nasser, G. V. Persiano, and A. Cusano, "Advanced cure monitoring by optoelectronic multifunction sensing system," *Thin Solid Films* **450**(1), 191–194 (2004).
11. S. Pu, X. Chen, Y. Chen, W. Liao, L. Chen, and Y. Xia, "Measurement of the refractive index of a magnetic fluid by the retroreflection on the fiber-optic end face," *Appl. Phys. Lett.* **86**(17), 171904 (2005).

12. C. B. Kim and C. B. Su, "Measurements of the refractive index of liquids at 1.3 and 1.5 micron using a fiber-optic Fresnel ratio meter," *Meas. Sci. Technol.* **15**(9), 1683–1686 (2004).
13. A. K. Nair, V. R. Machavaram, R. S. Mahendran, S. D. Pandita, C. Paget, C. Barrow, and G. F. Fernando, "Process monitoring of fibre reinforced composites using a multi-measurand fibre-optic sensor," *Sens. Actuat. B* **212**, 93–106 (2015).
14. D. Prada, C. Martelli, C. C. Kato, A. M. B. Braga, and M. S. P. Gomes, "CO<sub>2</sub> phase study using an optical fiber refractometer," *Proc. SPIE* **7753**, 775366 (2011).
15. G. Burton, L. Melo, S. Warwick, M. Jun, B. Bao, D. Sinton, and P. Wild, "Fiber refractometer to detect and distinguish carbon dioxide and methane leakage in the deep ocean," *Int. J. Greenh. Gas Control* **31**, 41–47 (2014).
16. E. J. Fordham, A. Holmes, R. T. Ramos, S. Simonian, S. M. Huang, and C. P. Lenn, "Multi-phase-fluid discrimination with local fibre-optical probes: I. Liquid/liquid flows," *Meas. Sci. Technol.* **10**(12), 1329–1337 (1999).
17. J. Zou, L. Ye, J. Ge, and C. Zhao, "Novel fiber optic sensor for ice type detection," *Measurement* **46**(2), 881–886 (2013).
18. A. D. Wallace, M. Boerkamp, P. Lye, D. W. Lamb, W. Doherty, and C. Fellows, "Assessment of an intrinsic optical fiber sensor for *in situ* monitoring of scale-forming salts," *Ind. Eng. Chem. Res.* **47**(4), 1066–1070 (2008).
19. J. D. Toner, D. C. Catling, and B. Light, "The formation of supercooled brines, viscous liquids, and low-temperature perchlorate glasses in aqueous solutions relevant to Mars," *Icarus* **233**, 36–47 (2014).
20. T. Mizunami, H. Tatehata, and H. Kawashima, "High-sensitivity cryogenic fiber-Bragg grating temperature sensors using teflon substrates," *Meas. Sci. Technol.* **12**, 914–917 (2001).
21. A. Chiuchiolo, M. Bajko, J. C. Perez, H. Bajas, M. Consoles, M. Giordano, G. Breglio, and A. Cusano, "Fiber Bragg grating cryosensors for superconducting accelerator magnets," *IEEE Photonics J.* **6**(6), 1–10 (2014).
22. D. Lee, R. Haynes, and D. J. Skeen, "Properties of optical fibres at cryogenic temperatures," *R. Astron. Soc.* **326**(2), 774–780 (2001).
23. V. R. Machavaram, L. Wang, S. D. Pandita, S. Hellmann, F. N. Bogonez, and G. F. Fernando, "Multi-point monitoring of cross-linking reactions," *J. Appl. Polym.* **131**(22), 1–11 (2014).
24. H. E. Johns and J. O. Wilhelm, "The refractive indices of liquid oxygen, nitrogen and hydrogen," *Can. J. Res.* **15a**(7), 101–108 (1937).
25. J. Badoz, M. L. Liboux, R. Nahoum, G. Israel, F. Raulin, and J. P. Torre, "A sensitive cryogenic refractometer. Application to the refractive index determination of pure or mixed liquid methane, ethane, and nitrogen," *Rev. Sci. Instrum.* **63**(5), 2967–2973 (1992).
26. G. Abbate, U. Bernini, E. Ragozzino, and F. Somma, "The temperature dependence of the refractive index of water," *Appl. Phys. (Berl.)* **11**, 1167–1172 (1978).
27. I. Thormahlen, J. Straub, and U. Grigull, "Refractive index of water and its dependence on wavelength, temperature and density," *J. Phys. Chem.* **14**, 933 (1985).
28. G. N. Ramachandran and T. Radhakrishnan, "The relation between thermo-optic and piezo-optic phenomena in crystals," *Philos. Mag.* **43**(338), 317–326 (1952).
29. W. B. Bald, "On crystal size and cooling rate," *J. Microsc.* **143**(1), 89–102 (1986).
30. D. H. Rasmussen and A. P. MacKenzie, "Clustering in supercooled water," *J. Chem. Phys.* **59**(9), 5003–5013 (1973).
31. G. P. Johari and S. J. Jones, "Infrared polarisability of hexagonal ice," *Nature* **263**(5579), 672–673 (1976).
32. W. Wagner, A. Saul, and A. Prub, "International equations for the pressure along the melting and along the Sublimation curve of ordinary water substance," *J. Phys. Chem.* **23**, 524–527 (1994).
33. D. G. Archer and R. W. Carter, "Thermodynamic properties of the NaCl + H<sub>2</sub>O system. 4. Heat capacities of H<sub>2</sub>O and NaCl(aq) in cold-stable and supercooled states," *J. Phys. Chem. B* **104**(35), 8563–8584 (2000).
34. P. V. Hobbs, *Ice Physics* (Oxford University 1974), Chap 5.
35. J. Workman, and L. Weyer, *Practical Guide to Interpretative Near-Infrared Spectroscopy* (CRC, 2007), Ch.6.
36. G. K. White, "Reference materials for thermal expansion: certified or not?" *Thermochim. Acta* **218**, 83–99 (1993).
37. J.G. Baust, and J.M. Baust, *Advances in Biopreservation* (CRC, 2007), Ch. 13.
38. M. Jakob and S. Erk, "Warmdehnung des eises zwischen 0 und –253°," *Z. Ges. Kalte-Ind.* **35**, 125–130 (1928).
39. C. A. Angell, "Liquid fragility and the glass transition in water and aqueous solutions," *Chem. Rev.* **102**(8), 2627–2650 (2002).
40. M. V. Mironenko, G. E. Boitnott, S. A. Grant, and R. S. Sletten, "Experimental determination of the volumetric properties of NaCl solutions to 253K," *J. Phys. Chem. B* **105**(41), 9909–9912 (2001).

## 1. Introduction

Monitoring and controlling crystallization of water has great importance in food [1], pharmaceutical [2], transportation [3], and aviation industries [4]. Water continues to be a subject of extensive research due to its intriguing molecular structures involved in polymorphism [5]. The pressure-temperature (P-T) phase diagram of water includes nine

stable forms and four metastable forms of crystalline ice; and two amorphous forms [6]. Major analytical techniques such as differential scanning calorimetry [7], cryo-optical microscopy, cryo-scanning electron microscopy, X-ray, infrared spectroscopy, nuclear magnetic resonance spectroscopy and magnetic resonance imaging serve to impart qualitative and quantitative information on the dynamics of crystallization which mainly involves nucleation and growth; size and shape of ice crystals and; spatial and temporal evolution of the crystallization process [1]. However, their usage is generally limited to laboratory environment and cost intensive. It is widely appreciated that optical fiber-based sensors enable remote monitoring of inaccessible and harsh environments due to their small size, chemical inertness and immunity to electromagnetic interference.

Amongst a variety of fiber sensors, the Fresnel reflection-based sensors serve as a low-cost means for chemical process monitoring. They are essentially based on monitoring the change in the refractive index of the medium in contact with the cleaved end of the fiber via the change in the intensity of normal Fresnel reflection of light. Unlike Bragg gratings and evanescent wave sensors, Fresnel sensors offer point-based measurements corresponding to the tip of the cleaved fibre and operate on relatively low-cost instrumentation. These sensors have been used extensively for monitoring the progression of cross-linking reactions in thermoset resin systems [8–10]; concentration and temperature of magnetic fluids [11]; and for measuring thermo-optic coefficients of liquids [12]. In conjunction with Fresnel reflection sensors, hybrid sensor designs based on Bragg gratings [10] and Fabry-Perot interferometric sensors enabled simultaneous measurement of parameters such as strain, temperature, refractive index and concentration of chemical species via appropriate signal decoupling schemes [13]. With reference to the storage and safety of CO<sub>2</sub> in geologic reservoirs, Prada *et al.* [14] reported on a Fresnel sensor-based refractive index monitoring to infer the phase of CO<sub>2</sub> as it is cooled from room temperature to –50 °C. Burton *et al.* [15] demonstrated discrimination of liquid CO<sub>2</sub> and supercritical methane bubbles using a Fresnel refractometer for deep ocean petroleum wells. An oblique cleave fiber end based on sensing refracted light intensity for discriminating multi-phase-fluid was also reported [16]. Zou *et al.* [17] demonstrated oblique cleave fiber-bundle-based probes for simultaneous detection of the ice type (glazed and rime) and the growth of ice layer via monitoring the reflected and scattered light intensities for aerospace applications. Exposed core plastic fiber-based evanescent field sensing was also used to infer the growth of crystals on the core via the changes in the attenuation of guided mode [18].

The work of Toner *et al.* [19] which reports on super-cooling of brines and the associated crystallization events from temperature information has motivated us to carry out the current investigations on the optical signatures of crystallization in conjunction with the temperature information. The current work is aimed at studying the crystallization of distilled water, and aqueous solution of NaCl using a Fresnel reflection fiber sensor as the liquids are subjected to rapid cooling using liquid nitrogen. These liquids play an important role in biological systems, food industry and transportation. Fused silica fiber-based sensors such as fiber Bragg gratings [20, 21] are particularly suitable for cryogenic environments because fused silica fibers are flexible even at cryogenic temperatures [22]. Fresnel sensors also offer scope for multipoint measurements to track the progression of crystallization with high spatial resolution. One of the authors of this work has reported previously on multiplexed Fresnel sensors for cure monitoring of thermoset resins [23]. To our knowledge at the time of writing, this work has not been reported.

## 2. Materials and method

### 2.1 Fiber sensor and interrogation

The optical fiber sensor system used in this study operates by monitoring the Fresnel reflection from the cleaved-end of a single-mode fiber (SMF 28 fiber). A fiber pigtailed

superluminescent diode (SLD1550S-A2, Thorlabs) with an output power of 2 mW and 3 dB bandwidth of 90 nm centered at 1550 nm was used as the light source. The SLD was driven by a laser diode driver and temperature controller (CLD1015, Thorlabs). The light reflected from the cleaved end of the fiber was measured using an InGaAs photodiode detector module (PDA10CS, Thorlabs) by means of a fiber optic circulator. The temperature of the test solutions was measured using k-type thermocouple. The photodiode and thermocouple signals were acquired simultaneously using NI 9219 data acquisition card housed in cDAQ 9171 chassis. A schematic of the experimental setup is shown in Fig. 1(a)-1(b).

## 2.2 Test solution

Distilled water and aqueous solution of sodium chloride (NaCl) formed the test media for the cooling experiments. The analytical reagent NaCl was supplied by SD Fine-Chem Limited, Mumbai. For the cooling experiments, NaCl solution of concentration 5.63 molal was prepared. The response of the fiber sensor was also measured over a concentration range of 0-6 molal of NaCl at room temperature.

## 2.3 Cooling setup

An expanded polystyrene cylindrical vessel of inner diameter 140 mm and wall thickness 20 mm was used as a container for liquid nitrogen (LN<sub>2</sub>). The open end of the polystyrene vessel was sealed using a polystyrene sheet on which a circular opening was made to accommodate the container of test solution. Two additional openings of smaller diameter were made to act as inlet for LN<sub>2</sub> and outlet for nitrogen gas. The container for test solution was a cylindrical stainless steel (SS304) vessel of inner diameter 47 mm, wall thickness 1.7 mm and length 120 mm. The pool of LN<sub>2</sub> surrounding the entire stainless steel vessel was meant for cooling the test solutions.

## 2.4 Sensor deployment

The SMF 28 fiber (8.2/125 μm) with 900 μm thermoplastic elastomer protective coating was inserted into the 1 mm bore of a hypodermic tube of length 87 mm. The coating was stripped using a mechanical stripper and the fiber was cleaved using a conventional fiber cleaver that produces a precise cleave angle of 0.5°. The cleave angle and clean fiber surface were ensured by examining the fiber under an optical microscope. The stripped length (17 mm) of the fiber was positioned outside the distal end of the hypodermic tube so that the jacketed length of the fiber remained inside the tube. The thermocouple was positioned adjacent to the fiber sensor at the same vertical height from the bottom of the vessel. The thermocouple and the hypodermic tube were secured in U-grooves made on parallel surfaces of a stainless steel bar via adhesive bonding. The steel bar was clamped to a manual XY-translation stage for alignment about the axis of the test solution container (SS vessel) to be enabled.

## 2.5 Method

All the cooling experiments were conducted at one atmospheric pressure (0.1 MPa) in laboratory environment. Prior to the cooling experiments involving solutions, the response of the sensor to immersion in a pool of LN<sub>2</sub> was investigated. The cleaved end of the fiber was immersed for short duration and then removed. A thermocouple was also used alongside the fiber sensor during the dip-in and take-out process. This process was repeated several times. Subsequently for cooling the solutions, the end of the fiber was positioned 10 mm from the base of the SS vessel and 50 ml of the solution was injected. Only the stripped length of the fiber and the thermocouple were immersed in the solution about the axis of the container. LN<sub>2</sub> was introduced into the polystyrene container through the inlet to fill the entire volume enclosing the SS vessel. The signals from thermocouple and the fiber sensor were acquired simultaneously. The signal from the fiber sensor in air and the test solution were obtained prior to cooling. The LN<sub>2</sub> gradually exhausted through the inlet and outlet of the polystyrene

lid. The experiment was continued until the test solution attained temperature close to the room temperature.

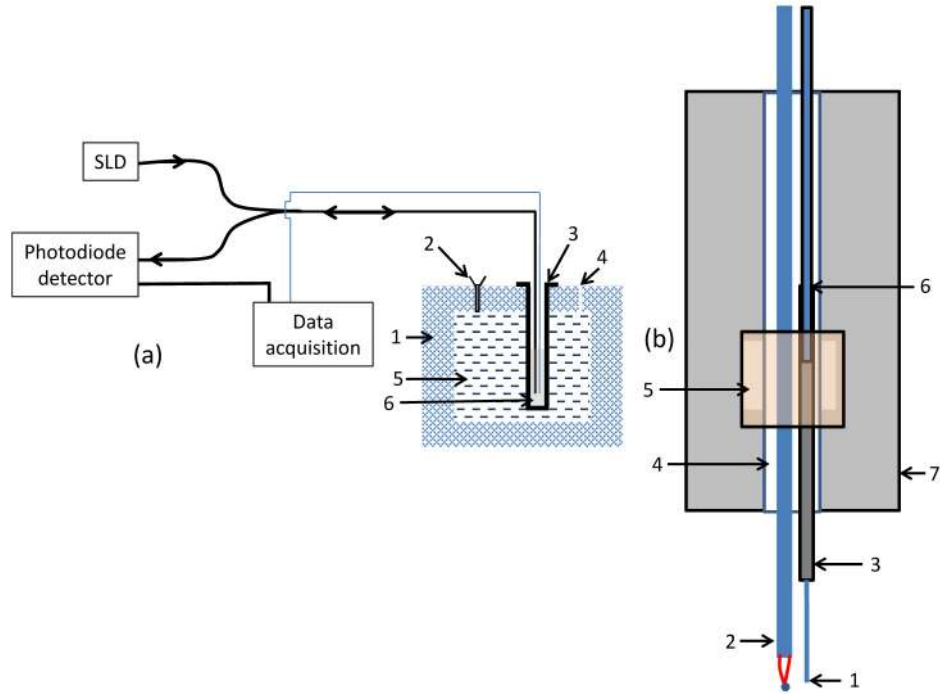


Fig. 1. (a-b): (a) Schematic experimental setup. (1) Polystyrene insulating container; (2) inlet for LN<sub>2</sub>; (3) SS vessel for containing the test liquid; (4) outlet for N<sub>2</sub>; (5) LN<sub>2</sub> pool; (6) test liquid. (b) Schematic of mounted thermocouple and fiber optic sensor; (1) Cleaved end of the fiber; (2) k-type thermocouple; (3) hypodermic tube; (4) U-shaped groove in SS bar; (5) adhesive bonding; (6) optical fiber with polymer jacket; (7) SS bar.

Initially, the tip of the thermocouple was positioned at a lateral separation of approximately 4-8 mm from the cleaved-end of the fiber sensor during the cooling experiments. Subsequently the temperature gradients inside distilled water were investigated using three thermocouples of which one was positioned close to the axis of the SS vessel; the second one at a lateral separation of 5 mm from the first; and the third one near the wall of the vessel. Finally, the fiber sensor and the thermocouple were deployed with a lateral separation of 2 mm; near the axis of the vessel and the cooling experiments with distilled water and NaCl solutions were carried out.

### 3. Results and discussion

#### 3.1 Monitoring solution concentration

The concentration of NaCl solution was incremented in steps of 1 molal up to 6 molal and the reflected signal from the optical sensor and the temperature were measured simultaneously over a period of time after complete dissolution. The refractive index of the solution was calculated using the method reported by Kim and Su [12]. The intensity of Fresnel reflection at normal incidence from the cleaved end of a single mode fiber can be used to obtain the refractive index of the medium in contact with the fiber. The refractive index of the medium (solution) ' $n_m$ ' in contact with the cleaved fiber end can be expressed as:

$$n_m = n_c \left[ \frac{1 - \frac{\Delta'}{\sqrt{R'}}}{1 + \frac{\Delta'}{\sqrt{R'}}} \right] \quad (1)$$

$$\Delta' = \frac{n_c - n_a}{n_c + n_a} \quad (2)$$

$n_c$  and  $n_a$  ( $= 1.00027$ ) are the refractive indices of the fiber core and air respectively; and  $R'$  ( $= V_a/V_m$ ) is the ratio of the measured voltages corresponding to the Fresnel reflections in air and the medium in contact respectively. The effective group index of refraction (EGIR) at 1550 nm for SMF-28 fiber is 1.4682. The refractive indices of the liquids used in these experiments are less than EGIR. Hence the change in their refractive index due to concentration and temperature variations are confined to the left arm of the parabola defined by the normal Fresnel reflectivity [9] of the fundamental mode at the boundary of cleaved end/liquid in contact. This implies that as the refractive index of the liquid increases/decreases, the Fresnel reflectivity decreases/increases as governed by the parabolic trend. However, small changes in liquid refractive index can be approximated to a linear fit. Figure 2 shows the plot of refractive index vs NaCl solution concentration, where the refractive index increases linearly at a rate of 0.0071 RIU/molal with the standard deviation of the refractive index values in the range of  $3.54 \times 10^{-5}$  -  $9.17 \times 10^{-5}$  over the specified concentrations. The refractive index of distilled water was found to be 1.327 at 29.6 °C.

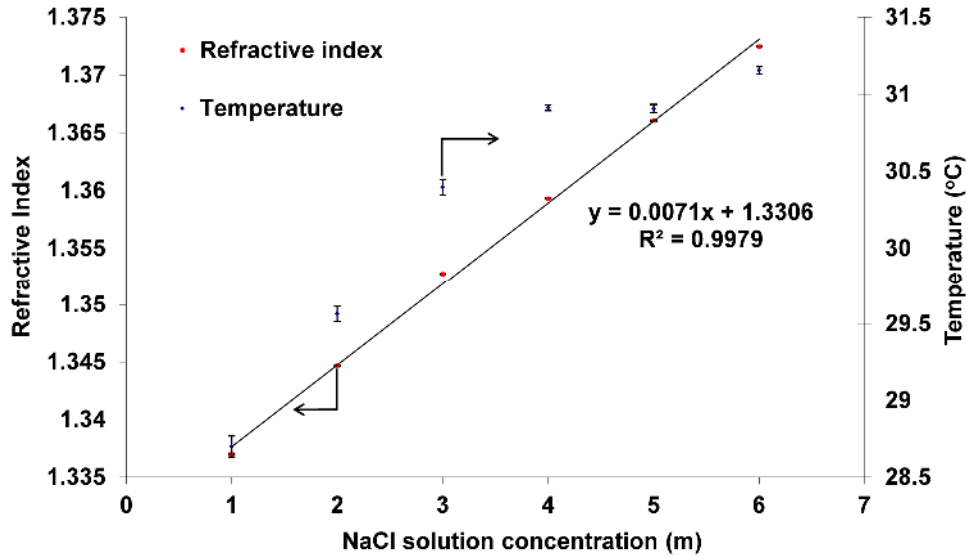


Fig. 2. Refractive index of NaCl solution obtained from the fiber sensor at different concentrations. Temperature variation during the measurement duration of refractive index is shown on secondary Y-axis. Ambient temperature ~30 °C.

### 3.2. Sensor immersion in LN<sub>2</sub>

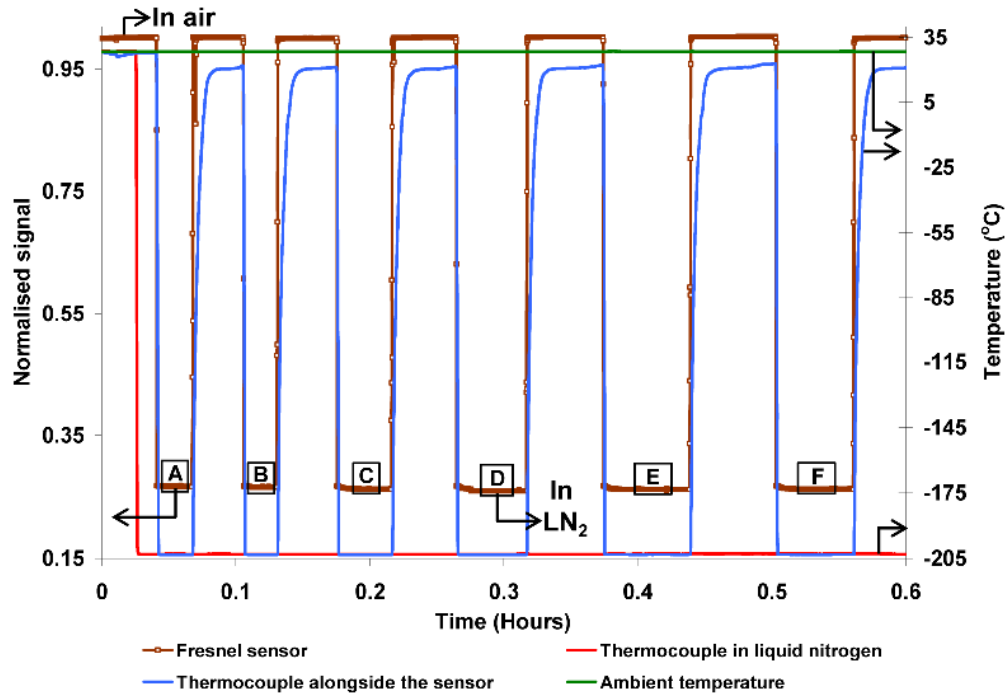


Fig. 3. Variations in detector signal due to immersion in LN<sub>2</sub> at  $-202\text{ }^{\circ}\text{C}$  during 6 cycles. Ambient temperature was  $\sim 28\text{ }^{\circ}\text{C}$ .

In Fig. 3 the detector signal was normalized with respect to the detector voltage in air at  $28\text{ }^{\circ}\text{C}$ , as indicated by a thermocouple constantly exposed to the laboratory ambient. A second thermocouple was immersed in LN<sub>2</sub>. The third thermocouple was positioned and secured alongside the fiber with the tip of the thermocouple and the cleaved end of the fiber at the same level with a lateral separation of few millimeters. They were dipped in a pool of LN<sub>2</sub> for some time and taken out into air gradually. The repeatability of sensor response and temperature data of the adjacent thermocouple is readily apparent from the 6 cycles of immersion as shown in Fig. 3. The average refractive index of LN<sub>2</sub> calculated using Eqs. (1) and (2) was found to be 1.2064, 1.2070, 1.2083, 1.2096, 1.2086 and 1.2083 with a standard deviation of  $\leq 10^{-4}$  as indicated by the domains A, B, C, D, E and F of the sensor signal during immersion in LN<sub>2</sub>. These results fairly agree with the previously reported LN<sub>2</sub> refractive index of 1.1990 [24] and 1.1985 [25]. The signal level in air subsequent to withdrawal from LN<sub>2</sub> during the cycles varied by a maximum of  $\sim 0.1\%$  as compared to that prior to the first immersion in LN<sub>2</sub>. The observed variations in index are probably due to condensation of minute amounts of atmospheric moisture at the end of the fiber when taken out of LN<sub>2</sub>. This signal level is significantly different from that due to immersion in bulk distilled water.

### 3.3. Distilled water

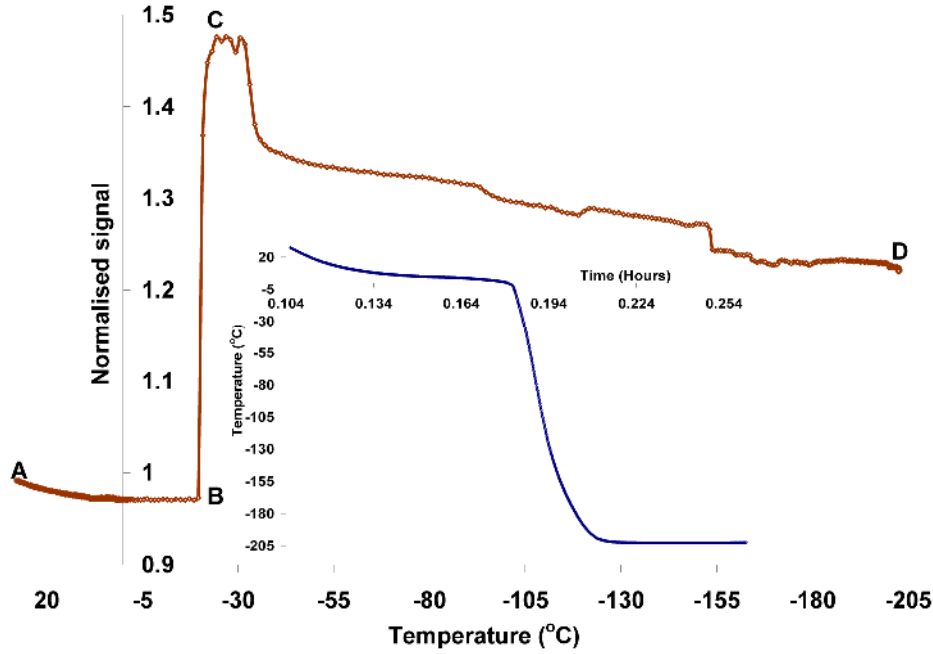


Fig. 4. Variations in detector signal during cooling of distilled water. The temperature on X-axis was measured using a thermocouple with a lateral separation of 4-8 mm. Ambient temperature was  $\sim 31$  °C.

**Table 1. Refractive index and temperature of distilled water at points shown in Fig. 4.**

	A	B	C	D
Temperature (°C)	27.28	-19.65	-24.4	-202
Refractive index	1.3283	1.3295	1.2993	1.3134

For all the cooling experiments, the Fresnel sensor signals were normalized with respect to the detector voltages corresponding to the Fresnel reflection from the liquid medium at room temperature before cooling. The refractive indices and temperatures corresponding to the points A, B, C and D in Fig. 4 are shown in Table 1. The corresponding temperature variation during cooling is shown in the inset of Fig. 4. The temperature decreased rapidly from  $-1$  °C at a rate of  $\sim 2.2$  °C/s.

Pure water crystallizes when cooled below  $0$  °C at one atmospheric pressure. The Fresnel reflection from the cleaved end of the fiber is mainly affected by temperature-induced changes in refractive index of water [26, 27]; phase transformation to ice; and the refractive index of ice, as the temperature is reduced from room temperature to  $-200$  °C. The Lorentz-Lorenz equation which describes the relation between refractive index ( $n$ ), density of scatters ( $M$ ) and polarizability of molecules ( $\alpha$ ) can be expressed as [28]:

$$\frac{n^2 - 1}{n^2 + 2} = \frac{4\pi}{3} M\alpha \quad (3)$$

In our experiments, as temperature ( $T$ ) is the driving factor that brings about the changes in the physical properties of water, the thermo-optic effect can be expressed as [28]:

$$\frac{dn}{dT} = -\gamma\rho \frac{dn}{d\rho} + \frac{(n^2 + 2)(n^2 - 1)}{6n} \Lambda_T \quad (4)$$

$$\frac{dn}{d\rho} = \frac{(n^2 - 1)(n^2 + 2)}{6n\rho} (1 - \Lambda_\epsilon) \quad (5)$$

$$\Lambda_T = \frac{1}{\alpha} \left( \frac{\partial \alpha}{\partial T} \right)_\rho \quad (6)$$

$$\Lambda_\epsilon = \frac{-\rho}{\alpha} \left( \frac{\partial \alpha}{\partial \rho} \right)_T \quad (7)$$

$\rho$  and  $\gamma (= -\rho^{-1} \cdot (d\rho/dT))$  represent density and volume expansion coefficient;  $\Lambda_T$  and  $\Lambda_\epsilon$  are the coefficients of temperature and strain polarizabilities respectively. Therefore the relative contributions of the first two terms in Eq. (4) and their signs determine the changes in thermo-optic of ice as it is cooled from 0 °C to -200 °C. From Table 1, the abrupt fall in the refractive index is due to the rate of crystallization of water via the nucleation and growth of stable crystal nuclei at the cleaved end of the fiber as governed by the rate of cooling. Bald [29] reported that high cooling rate and fast freezing front generate small crystal size. This suggests that the method of cooling employed and the volume of the distilled water in the cylindrical vessel can affect the structure of ice at the end of the fiber. Formation of ice at the cleaved end of the fiber changes the Fresnel reflectivity due to the accompanied change in refractive index. The density of ice at 0 °C is lower than that of water at 0 °C [30] and hence the refractive index decreases as implied by the abrupt rise in the signal. Johari and Jones [31] reported that the increase in infrared polarizability of water near 273 K was found to be associated with temperature-induced volume change rather than temperature explicitly. Therefore the abrupt rise in signal is due to the phase transformation of water to ice. Under atmospheric pressure and at relatively slow cooling rates, as in our experiments, ice is likely to exist in stable hexagonal crystalline form [32]. The temperature decreased rapidly from -1 °C (see Fig. 4(a) inset) as the ice formation is complete at the location of the thermocouple. Also, the specific heat of ice increases rapidly as temperature decreases below the crystallization temperature of water [33]. The gradual drop in the signal subsequent to abrupt rise corresponds to the densification of ice with lowering temperature [34] and hence the refractive index increased as the temperature reached -202 °C. However, the temperature corresponding to point B (see Fig. 4) was -19.65 °C which is much below the crystallization temperature of water. This discrepancy is probably due to the temperature gradient between the location of the thermocouple and the sensor. The temperature dependent near-infrared absorption of water and ice [35] could also have an influence on the rate of crystallization as light absorption at the end of the fiber can affect the cooling rate due to local heating. But this effect may not be significant owing to the fast cooling method employed.

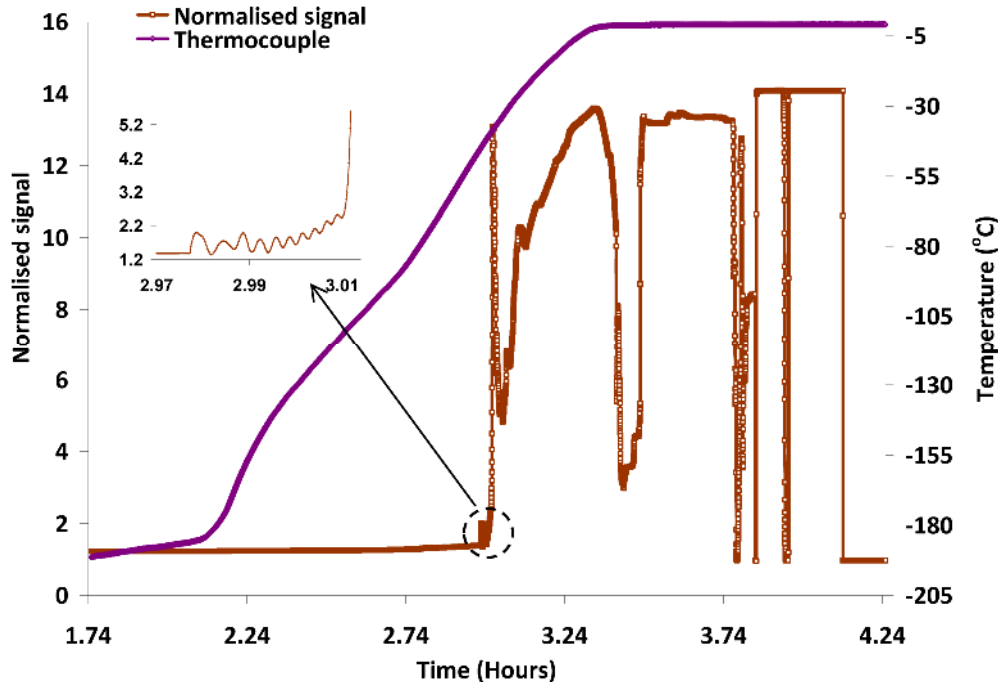


Fig. 5. Variations in the detector signal and temperature during heating of distilled water at laboratory ambient. The thermocouple and sensor have a lateral separation of 4-8 mm. Ambient temperature was  $\sim 31$  °C.

By the onset of heating phase, the  $\text{LN}_2$  in the polystyrene container was completely exhausted. Figure 5 was plotted against time to show the stable melting phase and the corresponding signal variations. The gradually increasing signal with temperature from  $-202$  °C indicates decreasing density of ice. Abrupt jumps and random variations in signal were observed even before the melting phase at  $-1$  °C commenced. The oscillations (see Fig. 5 inset) in the sensor signal at  $-45$  °C just prior to the abrupt rise in signal indicate possible involvement of a debonding mechanism between the fiber and ice which can be reasoned as follows: The thermal expansion coefficient of fused silica decreases in a non-linear fashion as the temperature decreases from  $7$  °C to  $-233$  °C [36]. From  $-113$  °C, thermal expansion coefficient turns negative and continues to decrease until  $-233$  °C. Thermal expansion coefficient of ice also decreases as the temperature decreases from  $0$  °C to  $-200$  °C [37, 38] but exceeds that of fused silica by two orders of magnitude. During the heating phase, ice exerts longitudinal extensive strain on the silica fiber. The difference between the thermal expansion coefficients of ice and silica increases linearly until  $-73$  °C and levels off with much smaller increase as the temperature increases from  $-73$  °C to  $-13$  °C. The increasing variation in thermal expansion coefficients in conjunction with the local density changes at the end of the fiber due to light absorption might have caused interfacial debonding between the cylindrical surface of the silica fiber and ice during the slow heating phase. This in turn could lead to debonding at the cleaved end of the fiber that caused a sudden rise in signal. The oscillations in the signal occur as a result of Fabry-Perot interference between the reflections from the end of the fiber and the light reflected in ice. The signal voltage corresponding to this abrupt rise (see Fig. 5 inset) is close to that obtained with the cleaved fiber in air and complies with the occurrence of debonding. During the melting phase at  $-1$  °C, the continuous transformation of ice to water causes light interaction with water and ice simultaneously that caused irregular signal variations. It was observed that the ice around the

thermocouple and fiber was surrounded by water in the vessel towards the end of the isothermal phase at  $-1\text{ }^{\circ}\text{C}$ . Subsequent to melting, the signal increased proportionally with temperature. Although the signatures of sensor debonding during the heating phase were observed in our repeat experiments, the temperature corresponding to debonding is not always the same.

### 3.4. Temperature gradients

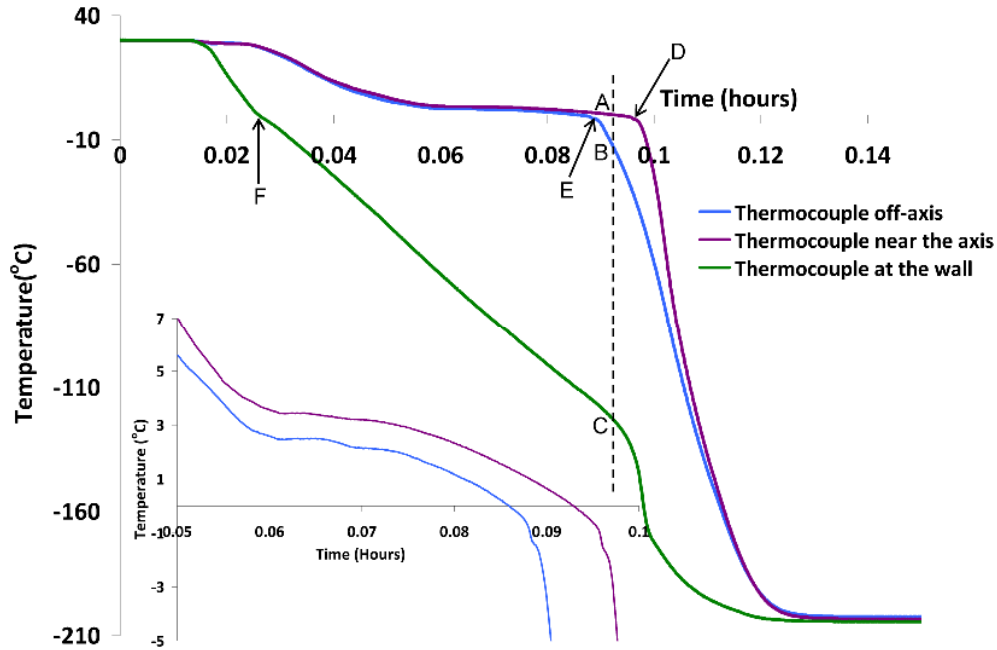


Fig. 6. Plot illustrating the temperature variation at different locations during cooling of distilled water. The near-axis and off-axis thermocouples have a lateral separation of 5 mm. Ambient temperature was  $\sim 31\text{ }^{\circ}\text{C}$ .

Table 2. Cooling rates and temperature at different points shown in Fig. 6.

	off-axis ( $^{\circ}\text{C}$ )	near-axis ( $^{\circ}\text{C}$ )	at wall ( $^{\circ}\text{C}$ )
A	-	0	-
B	-15.2	-	-
C	-	-	-124.3
Onset of rapid drop	-2.40	-2.71	-1.05
Rate of cooling ( $^{\circ}\text{C/s}$ )	-2.06	-2.99	-0.52

From the points of intersection of the vertical dotted line in Fig. 6, the temperatures corresponding to points A, B and C shown in Table 2 indicate temperature gradient between the near-axis and off-axis thermocouples with a separation of 5 mm. The inset in Fig. 6 is shown to illustrate the temperature variation during 0.05 to 0.1 hours. The temperatures corresponding to the onset of rapid drop as indicated by points D, E and F; and the subsequent cooling rates are also presented. Although the temperature at the wall drops to  $0\text{ }^{\circ}\text{C}$  at the earliest, the subsequent cooling rate is low because the heat extraction or transfer from within the entire volume of water via conduction occurs through the cylindrical surface and the base of the vessel. The evolution of cooling rate after point C, is due to diminished rate of heat flow through the wall followed by the thermal equilibrium of ice. These observations infer higher cooling rate near the axis of the vessel subsequent to crystallization. On the surface of the water, we observed ice formation from the vessel wall closing in radially towards the axis as the water around the axis solidified gradually to an opaque white solid with a convex

surface. A spiral-like curve was observed on the convex surface. The dynamics of warmer and colder water due to density changes in conjunction with the radially closing freezing front produces convex surface [39] during fast cooling. During the freezing process, we observed water circulating along the edge of the freezing ice front as it was closing in towards the axis. This circulation accompanied by simultaneous freezing produced a spiral-like structure over the convex surface. Photograph of the frozen distilled water ice surface is shown in Fig. 7.



Fig. 7. A photograph of frozen distilled water showing the convex surface and a spiral-like structure on it.

These observations confirm that the discrepancy in temperature corresponding to point B in Fig. 4 is due to temperature gradient between the thermocouple and the sensor location. Therefore smaller lateral separation can aid in better precision of temperature measurement at the end of the fiber with the current method of cooling.

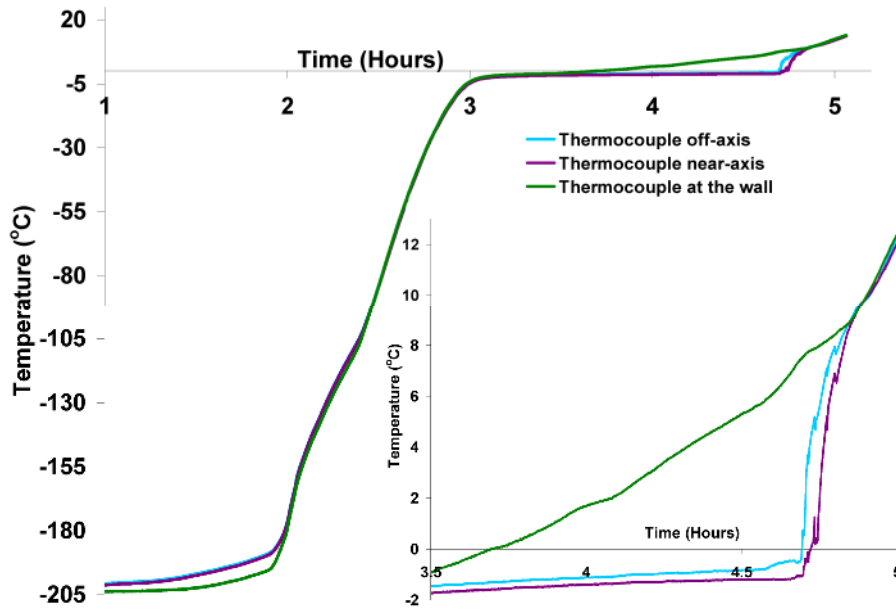


Fig. 8. Temperature variation from three thermocouples in distilled water during room temperature heating. The near-axis and off-axis thermocouples have a lateral separation of 5 mm. Ambient temperature was  $\sim 31$  °C.

Throughout the slow heating phase (see Fig. 8) at laboratory ambient, the on-axis and off-axis temperatures differed by  $<1$  °C until the end of dwell period at about  $-1$  °C. The melting first occurred at the wall as shown in the inset of Fig. 6 whilst the melting near the axis followed that of the off-axis location. These observations show that the temperature gradient between the on-axis and off-axis thermocouples is much smaller during the slow heating phase as compared to the fast cooling phase of the experiment. During the heating phase, it is therefore reasonable to assume that the temperature at cleaved end of the fiber and at a lateral separation of few millimeters do not differ significantly until the completion of the melting phase.

**Table 3. Refractive index and temperature data at points shown in Fig. 9.**

	A	B	C	D
Temperature (°C)	27.70	0.27	-1.55	-203.5
Refractive index	1.3281	1.3294	1.2961	1.3123

The abrupt rise in signal occurred at  $0.18$  °C (see Fig. 9, Table 3) is close to the crystallization temperature. The inset of Fig. 8 shows the rapid drop in temperature from  $-2$  °C. The spike in the signal is probably due to reflection from the freezing front approaching the cleaved end of the fiber. However, the magnitude of this spike will depend on local evolution of crystallization front and its orientation with respect to beam emerging from the fiber. Subsequently the signal dropped and continued to evolve in a similar fashion as in Fig. 4 with the formation of fiber/ice interface. Therefore it is apparent that temperature measurement at 2 mm lateral separation enables more precise estimation of temperature at the cleaved end of the fiber and correct interpretation of the onset and progression of crystallization.

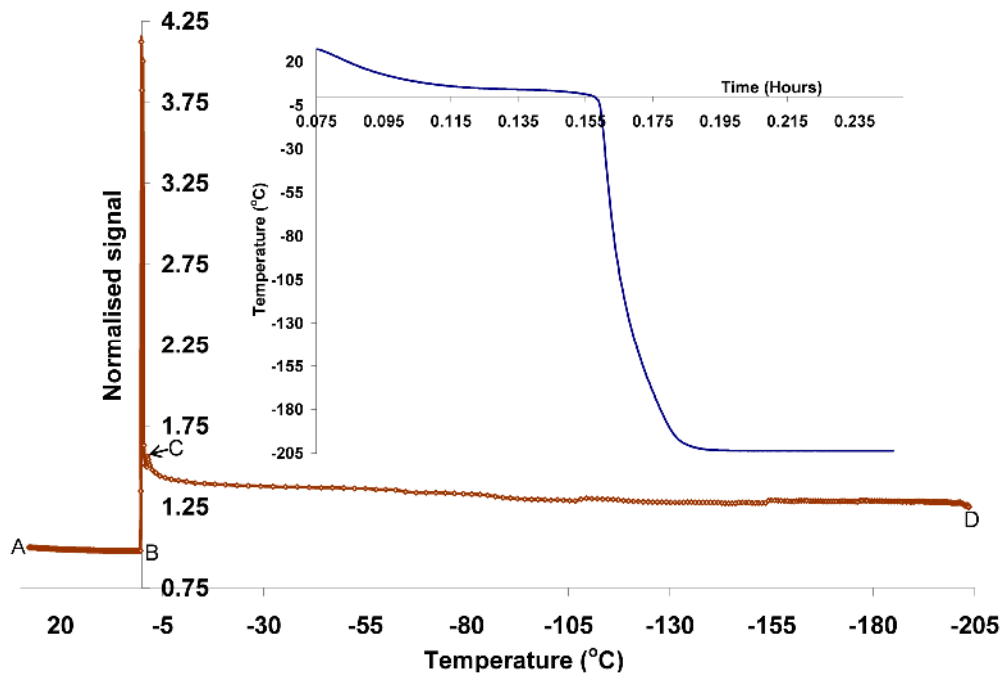


Fig. 9. Sensor signal and temperature variation during cooling of distilled water. The thermocouple and sensor have a lateral separation of 2 mm. Ambient temperature was  $\sim 30$  °C.

### 3.5. NaCl solution

According to the phase diagram of aqueous NaCl solution [19], the crystallization path way for 5.63 molal solution indicates that NaCl crystallizes as  $\text{NaCl}\cdot 2\text{H}_2\text{O}$  followed by the

crystallization of ice forming a eutectic mixture. From Fig. 10(a), the increase in index from A to B is due to temperature-induced densification of the solution [40]. The rapid drop in the signal from point B is followed by small variations leading to point C after which the signal increased abruptly. The rapid drop in temperature (see Fig. 10 inset) occurred from  $-30\text{ }^{\circ}\text{C}$  at a rate of  $3\text{ }^{\circ}\text{C/s}$ .

The Fresnel reflectivity changes as  $\text{NaCl}\cdot 2\text{H}_2\text{O}$  crystallizes from the solution. This phase separation event is accompanied by the release of heat and decrease in the concentration (see Fig. 2) of the solution. This tends to decrease the refractive index whilst the formation of  $\text{NaCl}\cdot 2\text{H}_2\text{O}$  at the end of the fiber appears to increase the refractive index (see Table 4). These counteracting effects determine the signal evolution from points B to C as governed by the rate of cooling.

Given the method of cooling, the rapid heat extraction quickly led to crystallization of ice. The signal transition from C to D can be attributed to the formation of eutectic mixture of ice and  $\text{NaCl}\cdot 2\text{H}_2\text{O}$ . This abrupt increase is similar to that observed during the crystallization of water (see Figs. 4 and 9). Further decrease in temperature leads to the densification of the eutectic mixture. The signal settled at an index of 1.3585 at  $-203\text{ }^{\circ}\text{C}$  and remained stable until the onset of the heating phase at laboratory ambient. Signal trends similar to that shown in Fig. 10(a) have been observed in the repeat experiments with the sensor positioned close to the axis of the vessel in conjunction with the current method of cooling and hence serve to impart the phase separation event of  $\text{NaCl}\cdot 2\text{H}_2\text{O}$  from the solution.

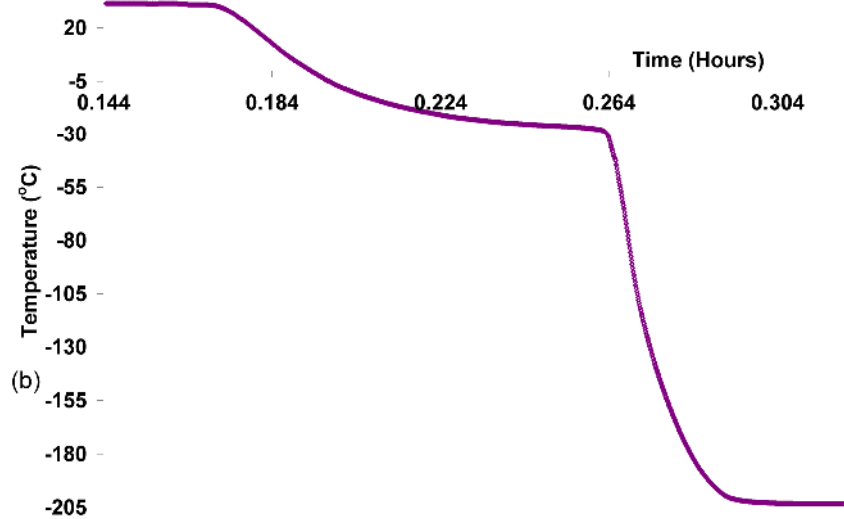
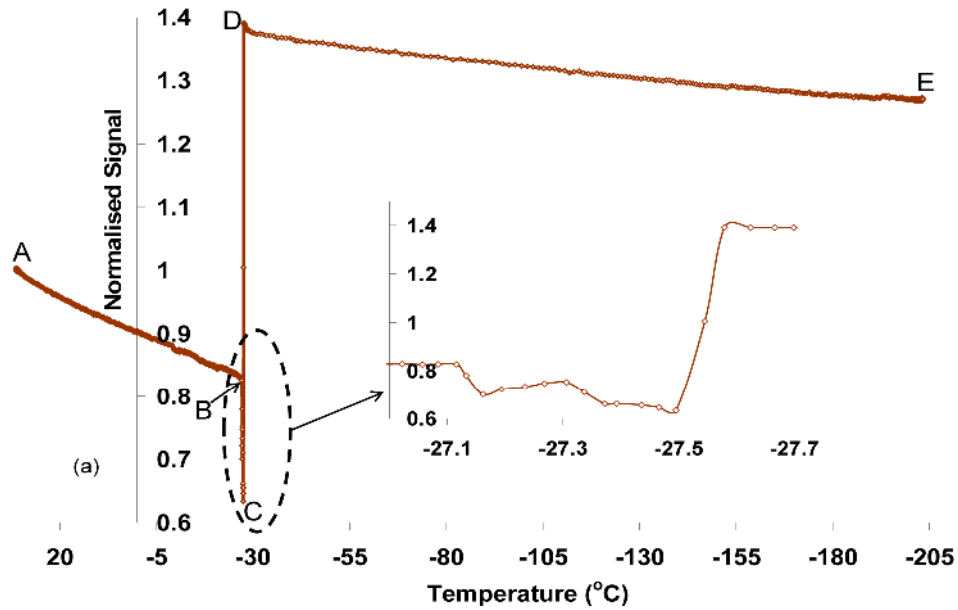


Fig. 10. (a-b). Sensor signal Vs temperature during the cooling of 5.63 molal NaCl solution. The thermocouple and sensor have a lateral separation of 2 mm. (b) Temperature variation with time. Ambient temperature was  $\sim 32^\circ\text{C}$ .

**Table 4. Refractive index and temperature of NaCl solution corresponding to the points shown in Fig. 10(a).**

	A	B	C	D	E
Temperature ( $^\circ\text{C}$ )	31.33	-27.11	-27.49	-27.57	-203.29
Refractive index	1.3704	1.3790	1.3898	1.3535	1.3584

However, the thermocouple does not infer the heat of crystallization of  $\text{NaCl}\cdot 2\text{H}_2\text{O}$  as a distinct temperature rise due to the rapid cooling effect unlike that observed by [19] during their slow cooling experiments. We also observed radial dependence of cooling rate which is similar to that of distilled water (see Fig. 6) but with the rapid drop in temperature occurring from  $-30^\circ\text{C}$ . It is therefore reasonable to expect variation in the signal trend with the cooling rate and the concentration of the solution.

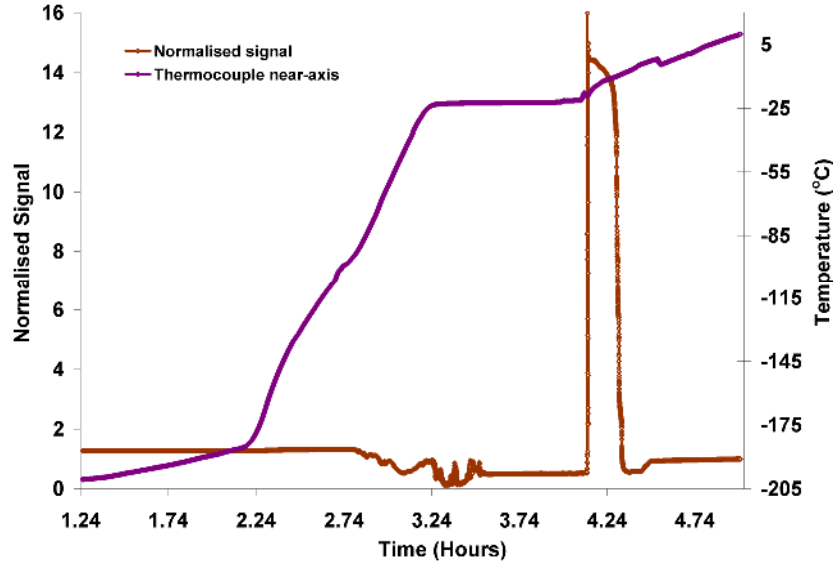


Fig. 11. Sensor signal and temperature variation during heating at laboratory ambient. The sensor and thermocouple have a lateral separation of 2 mm. Ambient temperature was  $\sim 32^\circ\text{C}$ .

During the heating phase (see Fig. 11), a gradual but small increase in signal was observed until  $-91^\circ\text{C}$  above which the signal experienced irregular variations as the temperature increased towards the stable eutectic temperature of  $-22.4^\circ\text{C}$ . This implies that the NaCl solution was supercooled by about 6 to 8  $^\circ\text{C}$  below the eutectic temperature. The stable domain of the signal during the eutectic phase was followed by an abrupt rise probably due to the debonding effect as mentioned previously. The end of the eutectic phase marks the transformation of eutectic mixture to solution form after which the signal increased with temperature. Although these signal features were observed in our repeat experiments, their occurrence with respect to temperature was not reproducible.

#### 4. Conclusions

A low-cost Fresnel reflection-based fiber sensor system has been demonstrated for detecting the crystallization of distilled water; and phase separation events in aqueous NaCl solution as they are cooled. The rapid cooling of NaCl solution swamps the exothermic signatures of crystallization and renders the thermocouple unsuitable for the detection of phase separation event. However, the fiber sensor signal clearly imparts the information on phase separation and formation of eutectic mixture. The experimental results demonstrate that the kinetics of crystallization at different cooling rates can be inferred from the sensor response. It is envisaged that in situations where the deployment of thermocouple in the proximity of the sensor is unviable, a temperature sensing element such as a fiber Bragg grating can be used. These sensors also offer an excellent scope for multiplexing and remote monitoring of multiple locations with potential applications in the areas such as bio-preservation, polymer processing and water quality monitoring. They can also aid in furthering the understanding of physical and chemical properties associated with the polyamorphic forms of water.

#### Acknowledgments

We are very grateful to VIT University for funding this research under RGEMS scheme. VRM would like to thank Professor Gerard F Fernando of University of Birmingham, UK for valuable discussions and Dr Krishna Mukharji Talasila for his assistance. The encouragement and support of Professor V Raju and Professor G Ramachandra Reddy is duly acknowledged.